AGU PUBLICATIONS

JGR

Journal of Geophysical Research: Oceans

RESEARCH ARTICLE

10.1002/2017JC012814

Special Section:

Oceanic Responses and Feedbacks to Tropical Cyclones

Key Points:

- The AE (CE) is divergence (convergence) of warm and fresh water, which can modulate the horizontal mass and heat transports
- The inflow of warm water weakened the SST cooling in CEs, which leads to the observed SST cooling in CEs much less than modeled
- The secondary cooling center locates at 100 m depth in the anticyclonic eddies and 350 m depth in the cyclonic eddies

Correspondence to:

L. Sun,
sunl@ustc.edu.cn or
sunl@ustc.edu

Citation:

Liu, S.-S., L. Sun, Q. Wu, and Y.-J. Yang (2017), The responses of cyclonic and anticyclonic eddies to typhoon forcing: The vertical temperature-salinity structure changes associated with the horizontal convergence/divergence, *J. Geophys. Res. Oceans*, *122*, doi:10.1002/2017JC012814.

Received 20 FEB 2017
Accepted 22 MAY 2017
Accepted article online 26 MAY 2017

The responses of cyclonic and anticyclonic eddies to typhoon forcing: The vertical temperature-salinity structure changes associated with the horizontal convergence/divergence

Shan-Shan Liu[1], Liang Sun[1,2], Qiaoyan Wu[2], and Yuan-Jian Yang[3]

[1]School of Earth and Space Sciences, University of Science and Technology of China, Hefei, Anhui, China, [2]State Key Laboratory of Satellite Ocean Environment Dynamics, Second Institute of Oceanography, State Oceanic Administration, Hangzhou, China, [3]Key Laboratory of Atmospheric Sciences and Satellite Remote Sensing of Anhui Province, Anhui Institute of Meteorological Sciences, Hefei, China

Abstract The responses of the cyclonic eddies (CEs) and anticyclonic eddies (AEs) to typhoon forcing in the Western North Pacific Ocean (WNPO) are analyzed using Argo profiles. Both CEs and AEs have the primary cooling at the surface (0–10 m depth) and deep upwelling from the top of thermocline (200 m depth) down to deeper ocean shortly after typhoon forcing. Due to the deep upwelling, part of warm and fresh water at the top of AEs move out of the eddy, which leads to a colder and saltier subsurface in the AEs after the passage of the typhoon. In contrast, the inflow of warm and fresh water heats and freshens the subsurface in the CEs to compensate the cooling induced by the typhoon. This explains why the observed strong SST cooling were much less than modeled, since the AEs are more frequent than CEs in the WNPO. It indicates that there is divergence (convergence) of warm and fresh water in the surface of AEs (subsurface of CEs). The divergence-convergence effects of the AEs and CEs lead to the secondary cooling center locate at a shallow layer of 100 m in the AEs and a much deeper layer of 350 m in the CEs. This shallow divergence-convergence flow could lead a shallow overturning flow in upper oceans, which may potentially influences the large-scale ocean circulations and climates.

Plain Language Summary The warm and fresh water diverges from anti-cyclonic eddies (AEs) but converges into the cyclonic eddies (CEs), in response to typhoon forcing. This explains why the observed strong SST cooling were much less than modeled, since the AEs are more frequent than CEs in the Western North Pacific Ocean. And it also shift the secondary cooling center to a shallow layer of 100 m in the AEs and to a much deeper layer of 350 m in the CEs. This shallow divergence-convergence flow could lead a shallow overturning flow in upper oceans, which may potentially influences the large-scale ocean circulations, biomass concentration and climates.

1. Introduction

The western North Pacific Ocean (WNPO) is a rich mesoscale eddy field (Figure 1). As the most vigorous motion in the ocean, the mesoscale eddies dominate the upper ocean kinetic energy with their kinetic energy about 2 order larger than that of the mean flow [*Pascual et al.*, 2006; *Xu et al.*, 2014]. They also make large-scale transports of heat, salt, and other tracers (e.g., nutrients) by trapping these passive tracers inside the eddies [*Bennett and White*, 1986; *Chelton et al.*, 2011; *McGillicuddy*, 2011].

The WNPO is also the most active typhoon (tropical cyclone) region. Typhoon typically produces intense oceanic entrainment and upwelling underneath the storm's center and relatively weaker and broader downwelling outside upwelled regions [e.g., *Price*, 1981; *Greatbatch*, 1984; *Cheng et al.*, 2015; *Jaimes and Shay*, 2015]. Typhoons can also make great impacts on the ocean flows by inputting mechanic energy to the ocean [e.g., *Liu et al.*, 2008; *Knaff et al.*, 2013], taking out huge heat energy from the ocean through their strong wind [*Sriver and Huber*, 2007; *Mei and Pasquero*, 2013; *Cheng et al.*, 2015], and cooling the sea surface temperature (SST) [*Price*, 1981; *Price et al.*, 1994; *Shay et al.*, 2000; *Sun et al.*, 2015]. The SST cooling induced by typhoons is mainly due to the entrainment of subsurface cold water, the air-sea flux counts only for

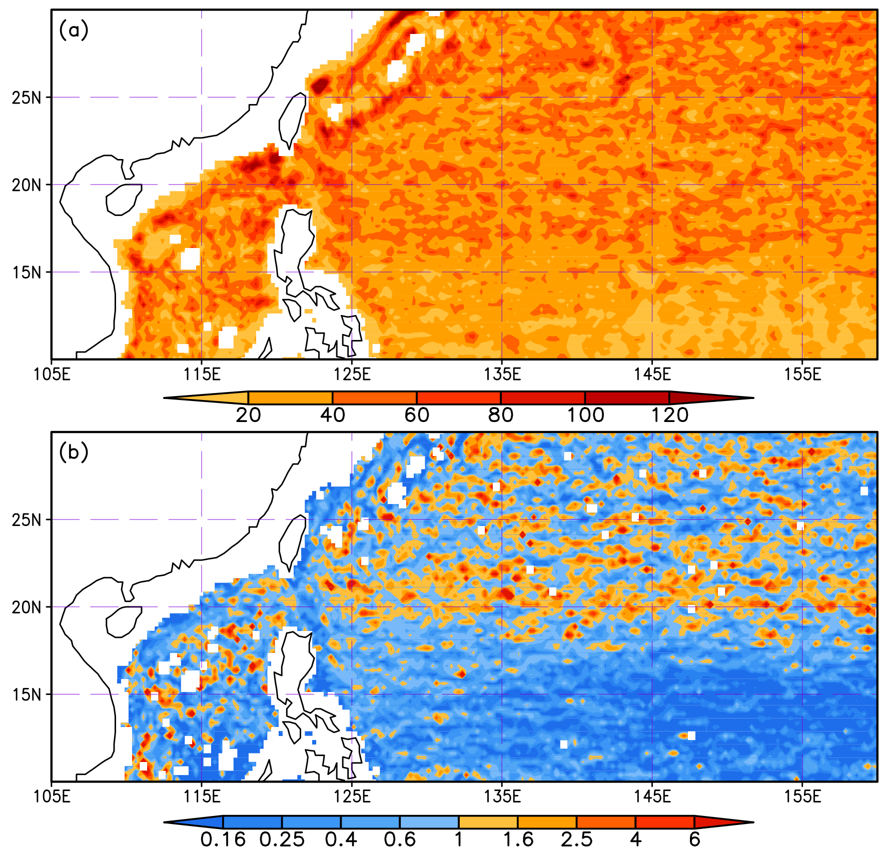

Figure 1. Statistics of annual eddy numbers in each 0.25° × 0.25° grid from 2001 to 2014 for (a) both CEs and AEs and (b) ratio of CEs to AEs.

about 5–15% [*Price*, 1981]. The entrainment of subsurface cold water can also induce phytoplankton blooming [*Lin et al*., 2003; *Sun et al*., 2010; *Foltz et al*., 2015]. In addition to the entrainment, the deep upwelling also can induce cooling the subsurface water above the thermocline (nearly the upper 200 m) according to the numerical simulations [e.g., *Jaimes and Shay*, 2015], which may induce a subsurface phytoplankton bloom stronger and longer than the surface bloom [*Ye et al*., 2013].

The mesoscale eddies, as main pretyphoon ocean features, can modulate the typhoon-ocean interactions in the tropical and subtropical regions [*Shay et al*., 2000; *Lin et al*., 2008; *Vincent et al*., 2012]. In general, they are classed into two types: the cyclonic eddy (CE) with negative sea level anomaly (SLA) and cold water in the core region, and the anticyclonic eddy (AE) with positive SLA and warm water in the core region. The AEs and CEs have different responses to typhoon. The relatively shallower warm water comparing to the background ocean environment in the CEs leads to a relatively unstable thermodynamic structure that easily elevates cold and nutrient-rich water below [e.g., *Walker et al*., 2005; *Zheng et al*., 2010; *Mei et al*., 2015]. Thus, the SST cooling and phytoplankton blooms induced by the typhoons are more pronounced in the CEs than in background [*Walker et al*., 2005; *Sun et al*., 2010]. Such enhanced SST cooling could in turn make a negative impact on the passing typhoons.

Although responses of significant SST cooling and phytoplankton blooms to typhoon forcing in the CEs were found in observations [*Walker et al*., 2005; *Sun et al*., 2010; *Zheng et al*., 2010] and numerical simulations [e.g., *Jaimes et al*., 2011; *Vincent et al*., 2013], both the observed strong surface cooling events and phytoplankton blooms were much less than expected [*Hanshaw et al*., 2008]. In the WNPO region, only 2 (Lupit and Ketsana) of 11 typhoons (18%) had notable impacts on SST cooling and phytoplankton blooms in 2003 [*Lin*, 2012]. In the period of 2000–2008, only about 10% of CEs were significantly influenced by super typhoons [*Sun et al*., 2014]. Although the typhoon characteristics (including intensity, translation speed, and size) [*Vincent et al*., 2012; *Mei et al*., 2015; *Lu et al*., 2016], typhoon forcing time [*Sun et al*., 2014], and ocean thermal stratification [*Walker et al*., 2005; *Zheng et al*., 2010; *Mei et al*., 2015] are important on oceanic responses. It seems that some important physical processes might be missed, which could weaken or compensate the typhoon-induced SST cooling in the CEs.

The case study of typhoon Namtheun (2004) provided a good example [*Sun et al*., 2012]. The water in the CE was freshened after typhoon forcing. The diagnosed fresh water (225 mm) was about twice of observed local extreme heavy rain (122 mm) induced by typhoon. It indicates that some warm and fresh water outside the CE moved into the CE. The CE induced by typhoon Fanapi (2010) experienced a similar process [*D'Asaro et al*., 2014]. The surface of the CE was trapped by a warm layer and thus becomes increasingly invisible in satellite SST measurements. These two cases imply that the surrounding warm and fresh water might weaken the SST cooling in the CEs after typhoon. It is still not know whether the process is unique to those two typhoons, or common processes to all CEs.

In the case of AEs, there is a predominantly downwelling, which favors vertically propagating inertial oscillation and downward energy propagation [*Jing and Wu*, 2014; *Guan et al*., 2014]. The deep warm water column can prevent significant cooling of the sea surface [*Jaimes and Shay*, 2015]. The huge heat content supply in the AEs can maintain or even intensify the passing typhoons [*Schade and Emanuel*, 1999; *Lin et al*., 2008]. The observed vertical structure of interior ocean responses to typhoons by using Argo profiles agrees with previous numerical simulations in general [e.g., *Price*, 1981; *Jaimes and Shay*, 2015], except that there were two observed cooling centers located at 100 and 350 m depth [*Cheng et al*., 2015]. These two weaker cooling centers were speculated to be linked to vertically propagating waves [*Cheng et al*., 2015]. However, the low time resolution (7–10 days) of Argo profiles hardly can capture such fast oscillation, other physical process must be involved.

The purpose of this paper is to evaluate the responses of AEs and CEs to typhoon forcing by a composite of the merged sea level anomaly (SLA) data and Argo data in the WNPO. A brief description of the data sets, typhoon model, and relative methods is presented in section 2. The oceanic eddy responses to typhoon forcing from surface down to thermocline of above 600 m depth are explored in detail in section 3. The associated studies and biomass responses are discussed in section 4. Finally, the conclusions are made in section 5.

2. Data and Method

2.1. SLA and Surface Current

The SLA data used here were from the merged and gridded satellite product of Maps of Sea Level Anomaly (MSLA), which were produced and distributed by AVISO (http://www.aviso.oceanobs.com/) based on TOPEX/Poseidon, Jason 1, ERS-1, and ERS-2 data. Currently, the products are available on a daily scale with a $0.25^\circ \times 0.25^\circ$ resolution in the global ocean. These data were corrected for all geophysical errors. In this work, the SLA data used were from 1 January 2001 to 31 December 2014. Recently, this data set was reprocessed as DUACS DT14 [*Pujol et al*., 2016].

The surface currents from a diagnostic data (SUCD) on a daily scale with a $0.25^\circ \times 0.25^\circ$ resolution in the global ocean is provided by Asia-Pacific Data-Research Center/International Pacific Research Center (APDRC/IPRC). The data were merged from four different data: AVISO sea level anomaly, Mean Dynamic Ocean Topography (MDOT), QuickSCAT wind, and Drifter trajectories. More detailed information on these data can refer to data sheet http://apdrc.soest.hawaii.edu/projects/SCUD/SCUD_manual_02_17.pdf.

2.2. Eddy Distribution

Using above SLA data (DUACS DT14), an eddy is defined as a simply connected set of pixels [*Wang et al*., 2003; *Chelton et al*., 2011] with a mononuclear conception [*Li et al*., 2014]. They are detected with watershed strategy and steepest descent algorithm for mesoscale eddy segmentation [*Li and Sun*, 2015]. The Genealogical Evolution Model (GEM) is further used to track the dynamic evolution of mesoscale eddies in the ocean [*Li et al*., 2016]. In the study, in order to exclude the major influence of the Kuroshio, we restrict the study area in 10–30°N, 105–160°E. The space distribution of annual mean eddies detected from 2001 to 2014 is showed in Figure 1. On average, there are about 40–60 eddies detected in each $0.25^\circ \times 0.25^\circ$grid in most region of the WNPO in each year, except for the coastal regions and the Kuroshio (Figure 1a). The AEs are more frequent than the CEs in the WNPO, especially at low latitudes (Figure 1b).

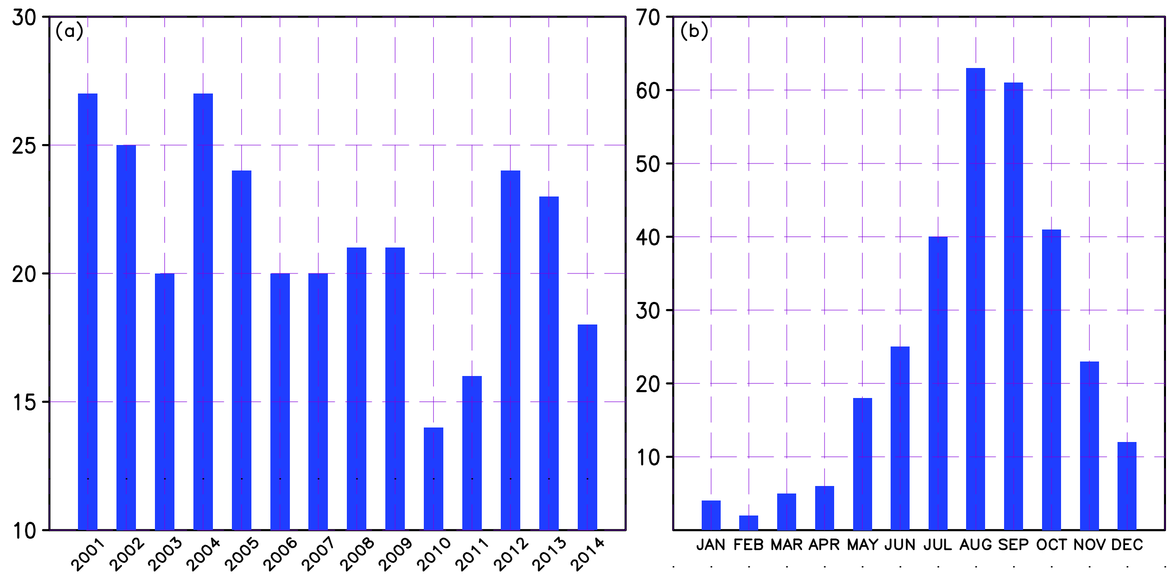

Figure 2. Typhoon numbers in each (a) year and (b) month.

2.3. Typhoon Data

The "best track data sets" of the WNPO used in this study from 2001 to 2014 were obtained from the Joint Typhoon Warning Center (JTWC). Each best-track file contains the tropical cyclone center locations, the central pressure, and the maximum sustained wind (MSW) speeds, the wind radius, and the radii of the specified winds (17, 25, 33, or 51 m/s) for four quadrants, at 6 h intervals. There are totally 85 tropical storms/tropical depression (TS/TD) events and 300 typhoons (Figure 2a) during this period. Only the typhoons are used in this study, and most of them occurred from July to September (Figure 2b).

The typhoon model used in this study is [e.g., *Mei et al.*, 2015]:

$$\begin{cases} V(r)=V_{max}\left(\dfrac{r}{R_{max}}\right), (r < R_{max}) \\ V(r)=V_{max}\left(\frac{r}{R_{max}}\right)^{-n}, (r \geq R_{max}) \end{cases} \tag{1}$$

where V_{max} and R_{max} are from the JTWC data. Instead to a fixed $n = 0.6$ [*Mei et al.*, 2015], the index n is estimated from the radii of the specified wind $n=-\ln\left(\frac{V_{25}}{V_{max}}\right)/\ln\left(\frac{r_{25}}{R_{max}}\right)$, where V_{25} and R_{25} are the velocity of 25 m/s and radii of 25 m/s in the track data. In order to get more accurate wind field of the typhoon, the typhoon track was linearly interpolated into 10 min interval before applying to the typhoon model.

2.4. Typhoon Works

To calculate the works from typhoon to the AEs and the CEs in the ocean, we first calculate the wind stress with:

$$\vec{\tau}=(\rho_a C_d U_{10} u, \rho_a C_d U_{10} v) \tag{2}$$

where ρ_a is the density of air (constant 1.25 kg/m^3) at sea level, U_{10} is the wind speed 10 m above sea level, u and v are the zonal and meridional components of the U_{10}, respectively, and C_d is the drag coefficient as [*Powell et al.*, 2003]:

$$C_d=\begin{cases} 1.2\times10^{-3} \quad U_{10} < 11\,m/s \\ (0.49+0.065\times U_{10})\times10^{-3} \quad 11 m/s \leq U_{10} \leq 25\,m/s \\ 2.115\times10^{-3} U_{10} \geq 25\,m/s \end{cases} \tag{3}$$

The total work input to ocean current $\vec{u}_c$ can be estimated as follows:

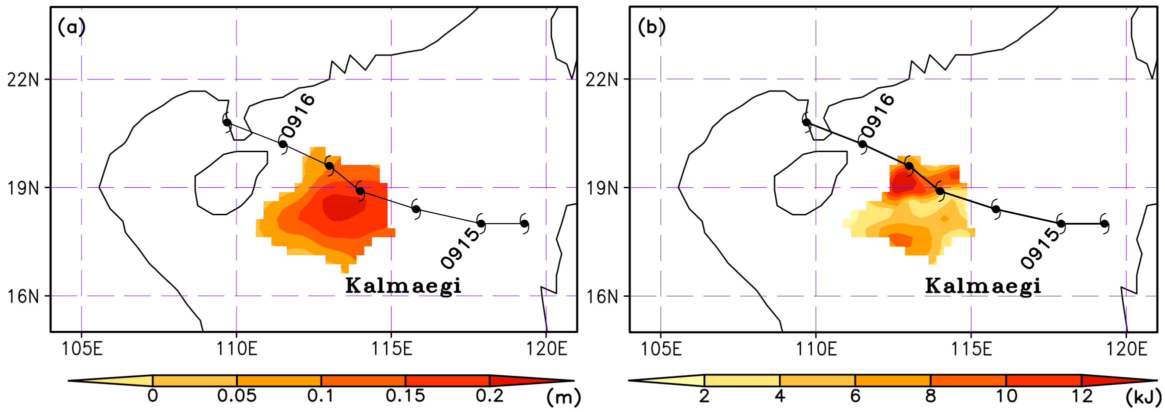

Figure 3. (a) The AE and the track of the typhoon Kalmaegi (2014). (b) The total work input into the current by typhoon.

$$W=\int \left|\vec{\tau}\cdot\vec{u}_c\ \right| dt \tag{4}$$

Typhoon Kalmaegi (2014) as an example is shown in Figure 3. Typhoon Kalmaegi (2014) passed over an AE in the northern South China Sea in September 2014 [*Zhang et al.*, 2016]. The AE located at the left side of the typhoon (Figure 3). The input work to ocean currents in the AE region by typhoon Kalmaegi is shown in Figure 3b.

In previous studies [e.g., *Sun et al.*, 2012; *Wu and Chen*, 2012; *Zhang et al.*, 2013; *Cheng et al.*, 2015; *Foltz et al.*, 2015; *Mei et al.*, 2015; *Wang et al.*, 2016], the region under the influence of typhoon is simply chosen according to the distance from typhoon center. In this study, the typhoon forcing region is chosen based on the typhoon work to the ocean current, so that both the distance from typhoon center and the typhoon forcing time are considered. In the WNPO, the typical total eddy kinetic energy (EKE) within subsurface water (200 m depth above) is estimated to be about 2 kJ/m^2 for typical average eddy velocity of 0.1 m/s [*Xu et al.*, 2014]. Here we choose the region of total work $W>1$ kJ/m^2 is as typhoon forcing region. Such work approximately equals to a gale of 17 m/s to an eddy current of 0.1 m/s for 6 h.

2.5. Argo Profiles

The Argo float profiles were extracted from the real-time quality-controlled Argo data base of China Argo Real-time Data center. The Argo data were collected and made freely available by the International Argo Project and the national programs that contribute to it. Argo profiles that are quality controlled are chosen in this study. To choose Argo profiles to study the ocean responses to typhoon forcing, we need consider not only the Argo locations relative to the typhoons but also the typhoon forcing.

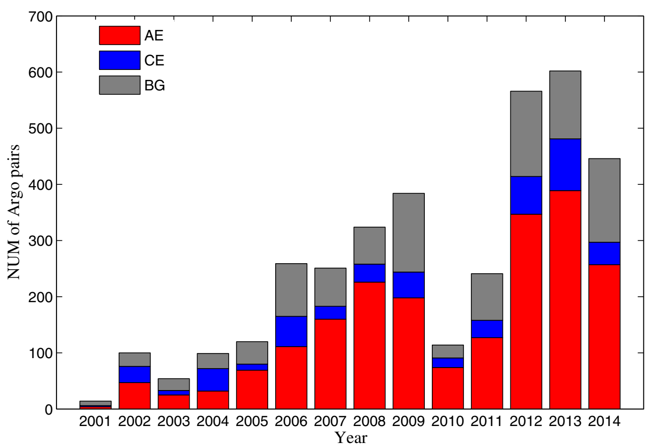

Figure 4. The Argo pairs in each year, where CE, AE, and BG represent cyclonic eddy, anticyclonic eddy, and background, respectively.

The Argo pairs used to calculate oceanic response to typhoons in eddies are chosen based on the following three criteria. First, the Argo pairs located at the typhoon forcing region defined previously within the same eddy. Second, the Argo pair includes two Argo profiles with time interval less than 10 days, one pretyphoon and the other posttyphoon. And the last, the zonal distance between two profiles is less than 0.25° and the meridional distance is less than 0.5°. The number of the chosen Argo pairs in each year is shown in Figure 4. Since the AEs are more frequent than CEs in the WNPO as shown in Figure 1, the

Argo pairs are more frequent in the AEs than CEs. There are about 500 pairs in the CEs, 2100 pairs in the AEs, and 1000 pairs in the background (regions without eddy).

2.6. Eddy Vertical Profiles

Since we focus on the eddy more than typhoon, we use eddy-center coordinate [*Zhang et al.*, 2013; *Wang et al.*, 2015] other than typhoon-center coordinate [*Wang et al.*, 2016] for composite analysis in this study. As a reference, the climatological composition of temperature, salinity, and density profiles of CEs, AEs, and background (BG) before typhoon forcing are shown in Figure 5. Each Argo profile was interpolated into given layers. The layers are 10 m each from surface to 200 m depth, and 20 m each from 200 to 600 m depth. In this study, what we consider is the variations of temperature and salinity. The composite of the data will largely reduce the noise and uncertainty in the data. In addition, we draw the conclusion only when both of the temperature and salinity independently present the similar results.

As shown in Figure 5, both temperature and density before the influence of typhoons are monotonic change with depth. But the salinity has a maximum at about 100 m depth. Such results are similar to previous observations in the Kuroshio extensions at 35–40°N, 160–165°E [*Dong et al.*, 2014]. Unlike in the Kuroshio extensions, the surface water is much fresher in the AEs than the CEs, and the contrary is true in the Kuroshio extensions. The main density difference between AEs and CEs exists at upper 200 m. The difference between AEs, CEs, and the background is very small below 200 m depth, where is main pycnocline or thermocline. Based on the climatological mean states of AEs and CEs under the influence of typhoon and the previous studies [e.g., *Jaimes and Shay*, 2015; *Sun et al.*, 2012; *Xu et al.*, 2014; *Zhang et al.*, 2016], the upper ocean in this study is separated into three continued parts: the surface (0–10 m depth), the subsurface (10–200 m depth), and the thermocline (200–600 m depth).

3. Results

3.1. Responses at Surface

When the typhoons passed over the ocean, there is SST (upper 10 m in this study) cooling after typhoon forcing. The distributions of Argo observed SST cooling in the CEs and AEs are shown in Figure 6 and summarized in Table 1. In the CEs, about 67% of the total samples show cooling after typhoon (Table 1).

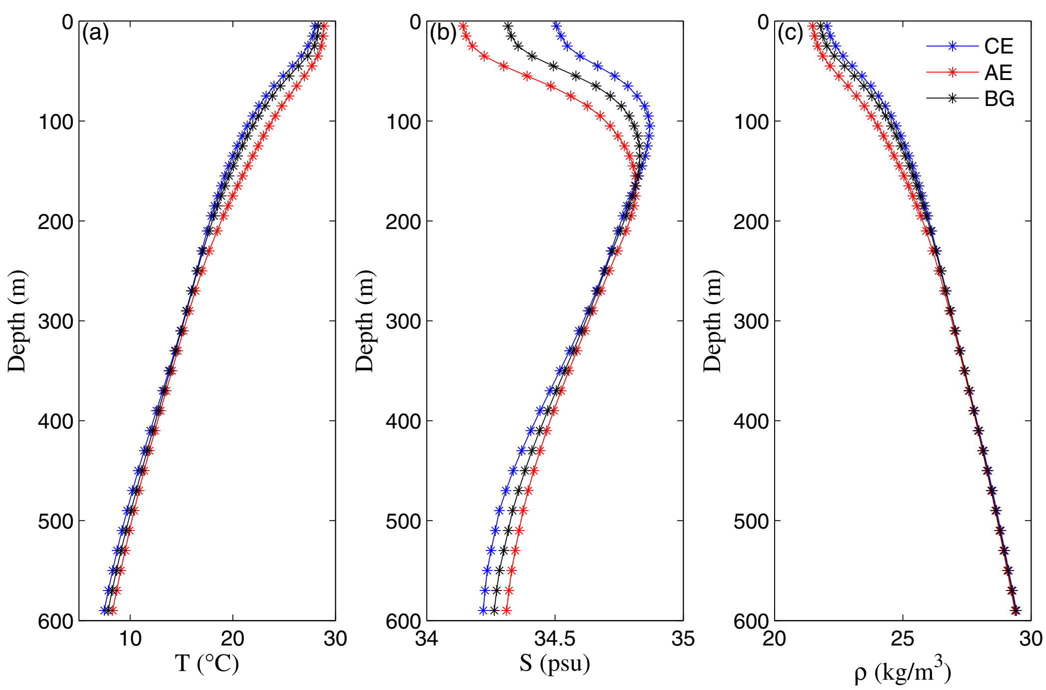

Figure 5. The mean profiles of temperature, salinity, and density from 2001 to 2014 in AE (red), CE (blue), and background (black) under the influence of typhoons.

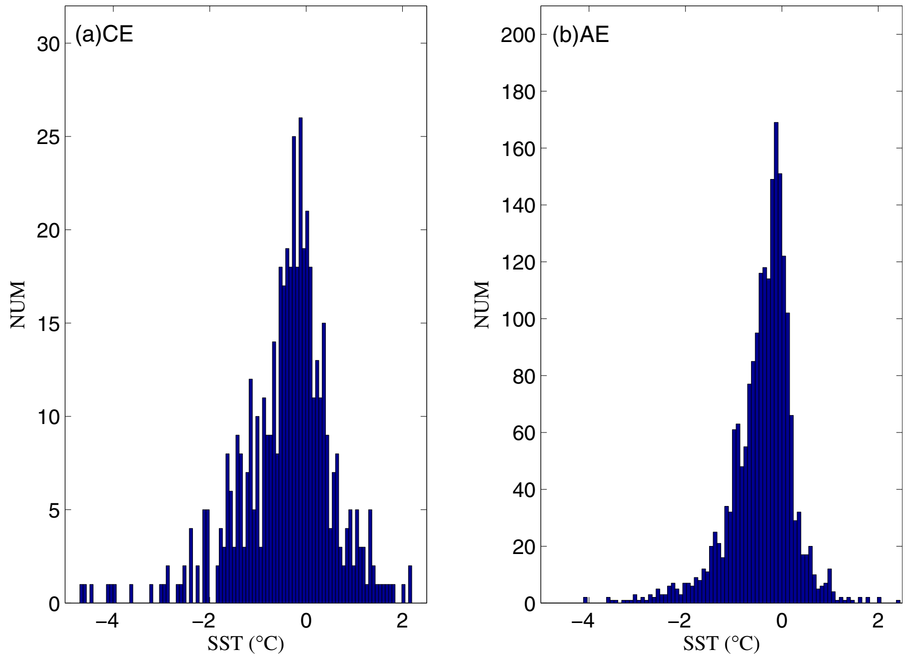

Figure 6. The probability density function (pdf) of SST change in Argo floats after typhoons for the (a) AEs and (b) CEs.

Twenty-two percentage of the Argo pairs observed significant cooling of <-1°C, and only 7% of the Argo pairs observed the strong cooling of <-2°C (Table 1). Such strong cooling had been observed in previous studies [*Lin et al*., 2003; *Sun et al*., 2010] due to the unstable thermodynamic structure in the CEs [*Walker et al*., 2005; *Sun et al*., 2012]. The mean of all cooling samples was -0.86°C, and the rest 33% of Argo pairs observed SST warming with a mean of 0.526°C. The warming samples reduced the total average SST cooling in the CEs to -0.408°C (Table 2). Comparing to the CES, the SST cooling was more frequently observed in the AEs (77% in Table 1). But the strong cooling (<-2°C) was rarely seen (1% in Table 1). Only 13% of the

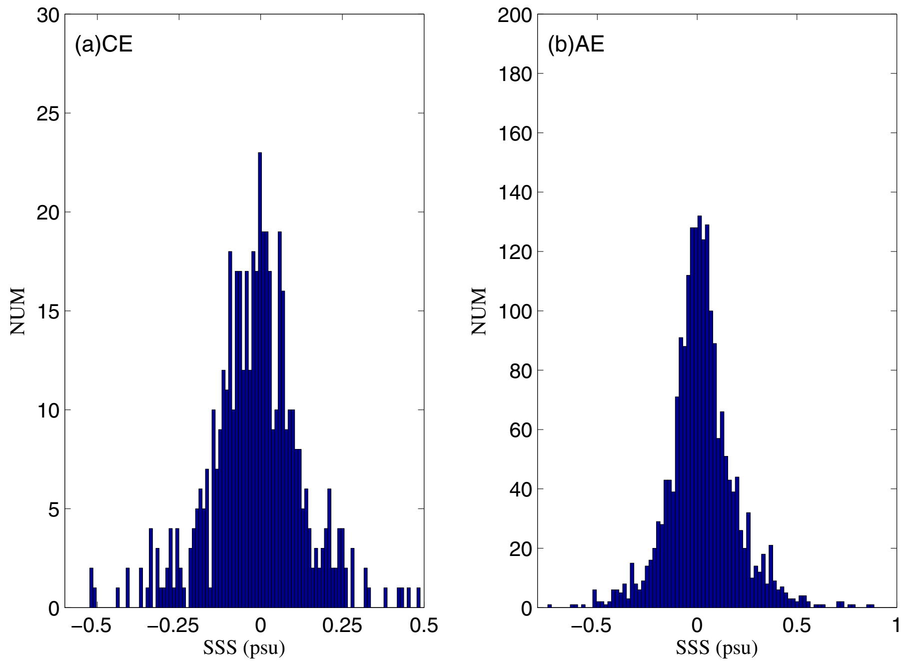

Figure 7. The pdf of SSS change in Argo floats after typhoons for the (a) CEs and (b) AEs.

Table 1. The Percentage and Means of Different Parts for ΔSST and ΔSSS in the CEs and AEs

	ΔSST					ΔSSS		
	<−2°C (Ratio)	<−1°C (Ratio)	<0°C (Ratio)	<0°C Mean	>0°C Mean	<0 psu (Ratio)	<0 psu Mean	>0 psu Mean
CE	7%	22%	67%	−0.860	0.526	55%	−0.110	0.099
AE	1%	13%	77%	−0.615	0.295	44%	−0.109	0.132

Argo pairs had observed significant cooling of <−1°C. The mean of cooling samples was −0.615°C (Table 1) and the total average SST cooling was −0.406°C (Table 2). It indicates that the SST cooling is weaker but more frequent in the AEs than in the CEs.

Both decreasing and increasing of sea surface salinity (SSS) are observed after typhoon's passage (Figure 7). In the CEs (Figure 7a), more than half (55%) of the SSS samples decreased with a mean of −0.11 psu, the others (45%) increased with a mean of −0.099 psu (Table 1). On average, the SSS decreased of 0.016 psu (Table 2). The observed SSS decreasing implies that the freshwater from typhoon precipitation leads the SSS change in CE.

While in the AEs (Figure 7b), the SSS changed in a different way. Forty-four percentage SSS samples decreased with a mean of −0.109 psu, and the rest (56%) increased with a mean of 0.132 psu (Table 1). The average SSS increased with 0.023 psu (Table 2). Two possible processes are response for the SSS increase. One is that the entrainment brings the subsurface salt water up to the surface and surface fresher water down to the subsurface. In this process, the SSS increases but subsurface salinity decreases. It does not change the whole vertical column salinity. The other is the evaporation due to strong typhoon wind, which takes fresher water from surface. This process increases the whole vertical column salinity. The increased SSS in the AEs indicates the SSS change due to the entrainment and evaporation is larger than that due to typhoon-induced precipitation.

3.2. Responses at Subsurface

To investigate the responses in eddies at subsurface, the budgets of heat and salinity are derived from the conservation of the bulk heat Q and bulk salinity S [e.g., *Sun et al.*, 2012],

$$\begin{cases} \dfrac{\partial Q}{\partial t} = -U \cdot \nabla Q - Q_e \\ \dfrac{\partial S}{\partial t} = -U \cdot \nabla S - S_e \end{cases} \tag{5}$$

where $U \cdot \nabla$ is the flux by horizontal advection and/or vertical flows, Q_s and S_e are the fluxes of heat and salt due to entrainment, respectively.

The responses of AEs and CEs to the typhoons at subsurface (10–200 m depth) are illustrated in Figure 8. For the subsurface temperature in the CEs (Figure 8a), it cooled only at a shallow layer about 30–40 m depth, but warmed at the rest layer of 40–200 m depth. The largest warming located at about 60–70 m depth. Such warming is mainly due to the entrainment of surface warm water [*Price*, 1981]. The average temperature change in whole subsurface water is about 0.016°C, which indicates net heat content gain (13 MJ/m^2) in the CEs (Table 2). Unlike in the CEs, the temperature cooled on whole subsurface water depth in the AEs. The average temperature change in whole subsurface water is about −0.15°C, which means net heat content loss (123 MJ/m^2) in the AEs (Table 2). Although the air-sea flux can be as large as 260 MJ/m^2 at certain small location for a category 5 typhoon [*Shay et al.*, 2000], the typical value of air-sea flux was quite

Table 2. The Average Changes of Heat and Salt in the CEs and the AEs, Where E-P Represents Fresh Water Flux (Evaporation Minus Precipitation)

	AE			CE		
	Surface (0–10 m)	Subsurface (0–200 m)	Thermocline (200–600 m)	Surface (0–10 m)	Subsurface (0–200 m)	Thermocline (200–600 m)
ΔT (°C)	−0.406	−0.150	−0.073	−0.408	0.016	−0.036
ΔH (MJ/m^2)	−17	−126	−123	−17	14	−60
ΔS (psu)	0.024	0.001	−0.004	−0.017	−0.010	−0.002
E-P (mm)	6.8	6.5	−41.8	−4.7	−59.7	−17.7

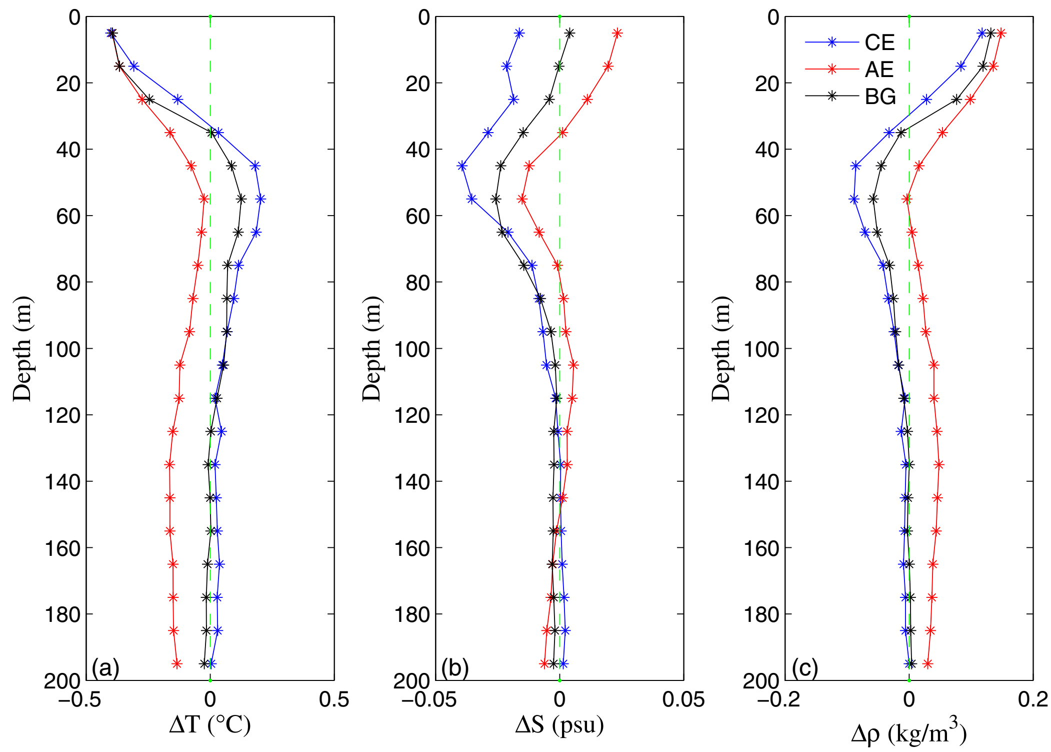

Figure 8. The mean vertical profile change of temperature, salinity, and density after typhoon at subsurface, where blue, red, and black present AE, CE, and background, respectively.

smaller, e.g., area average value of the whole forcing region is only about 20–30 MJ/m^2 [*Shay et al*., 2000] and 40 MJ/m^2 for a category 2 typhoon [*Sun et al*., 2012]. The annual mean of air-sea flux due to typhoon forcing on the global scale is 34 MJ/m^2 (11.05 w/m^2) [*Cheng et al*., 2015]. It implies that such huge subsurface heat content loss in the AEs cannot be simply due to the local air-sea interaction.

The subsurface salinity also varied in different ways in the AEs and CEs (Figure 8b). In the CEs, the water freshened significantly from the surface to 100 m depth. The average salinity decrease in subsurface water was about −0.01 psu (Table 2). Below 100 m, the salinity increased a little after typhoon's passage. The strong freshening of subsurface water implies some net fresh water input in the CEs. The salinity change was much more complicated in the AEs. The salinity increased above 40 m and at the depth between 100 and 140 m, but decreased on the rest subsurface water. On average, the total salinity increased about 0.001 psu within whole subsurface water of the AEs (Table 2).

The temperature and salinity changes lead to the density change after the typhoon's passage (Figure 8c). In the CEs, the water became lighter after typhoon mainly due to the freshening of water. In the AEs, the water became a little heavier due to the losing of fresh water and heat to atmosphere.

3.3. Responses at Thermocline

Unlike in the subsurface layer, the changes in the thermocline below 200 m are relatively similar in both CEs and AEs. As shown in Figure 9a, the water cooled about 0.036°C and 0.073°C in the CEs and AEs, respectively (Table 2). The only difference is that the maximum cooling occurred at 350 m in the CEs, whereas the maximum cooling occurred at subsurface of 100 m depth in the AEs. Previous study also identified the cooling center at 100 and 350 m depth [*Cheng et al*., 2015]. In this study, only two different cooling centers are detected in the CEs and AEs.

On average, the salinity in the layer below 200 m depth decreased about 0.0015 and 0.0036 psu in the CEs and AEs (Table 2), respectively, as shown in Figure 9b. Therefore, the deep water became fresher even without surface precipitation. As the temperature dominates the density variations of sea water, the density became a little heavier due to sea water cooling (Figure 9c).

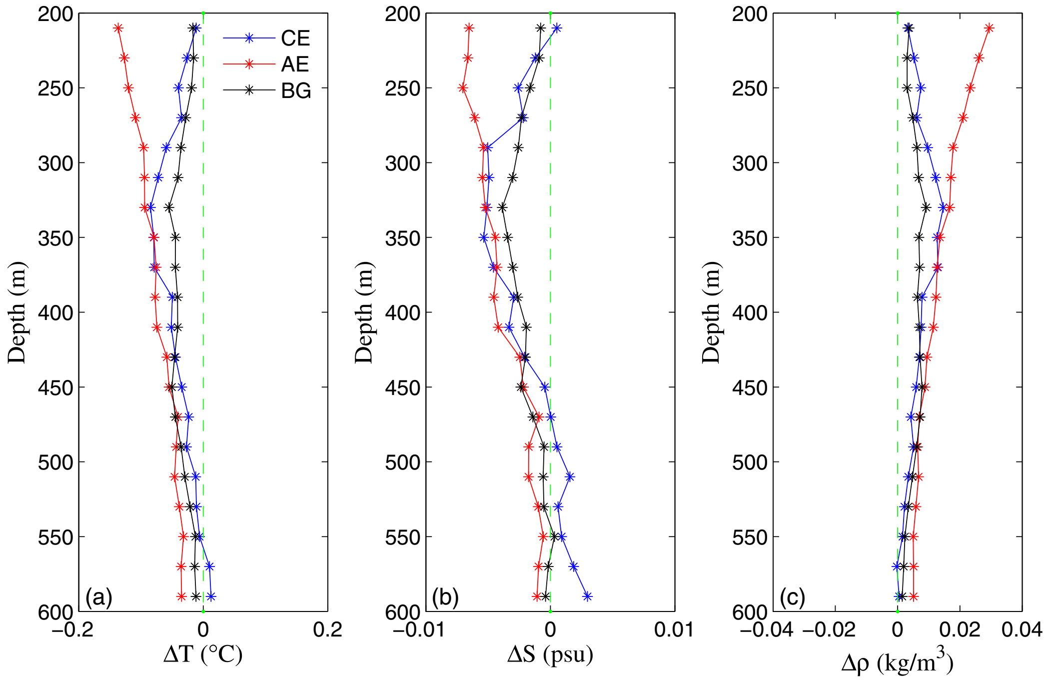

Figure 9. The same as Figure 8 but for water within thermocline (200–600 m depth).

3.4. Upwelling and Downwelling

The ocean responses to typhoon forcing involve complex dynamics in the upper ocean, which include air-sea flux exchanges, entrainment, upwelling and/or downwelling, etc. The T-S plots for the CEs and AEs are used to diagnose which process dominates the ocean responses (Figure 10). In the subsurface (200 m shallower), both the temperature and salinity changes are large (Figure 10a). The posttyphoon T-S curves shift away from the pretyphoon T-S curves from the surface to subsurface water. The stronger the nonadiabatic processes, the larger the shift distance of the curve. The largest shift locates at the surface, where both the

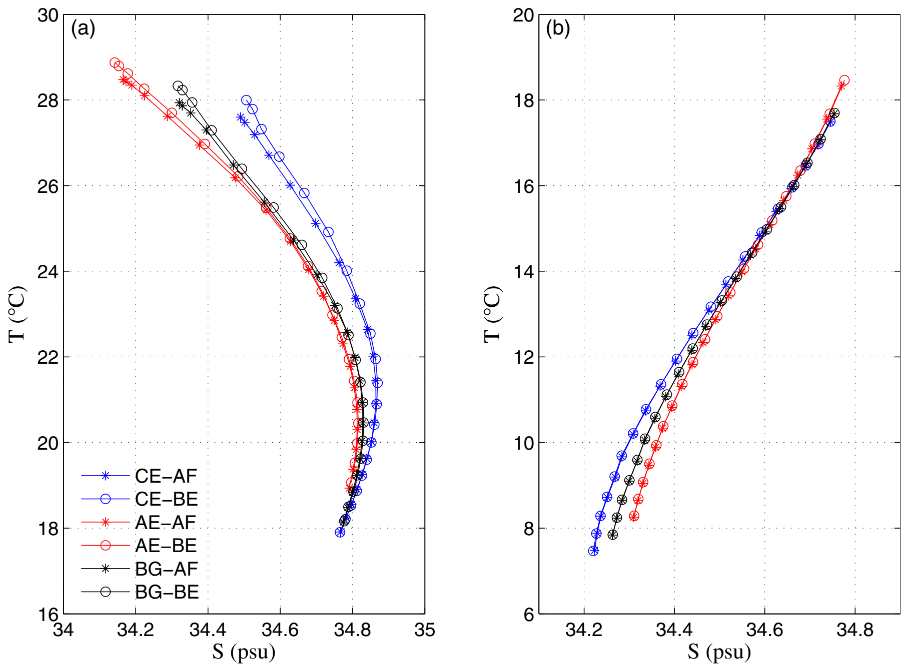

Figure 10. The T-S plot for AE (red), CE (blue), and background (black), (a) for surface to subsurface and (b) for subsurface to upper ocean. AF and BE mean after typhoon passage and before typhoon passage, respectively.

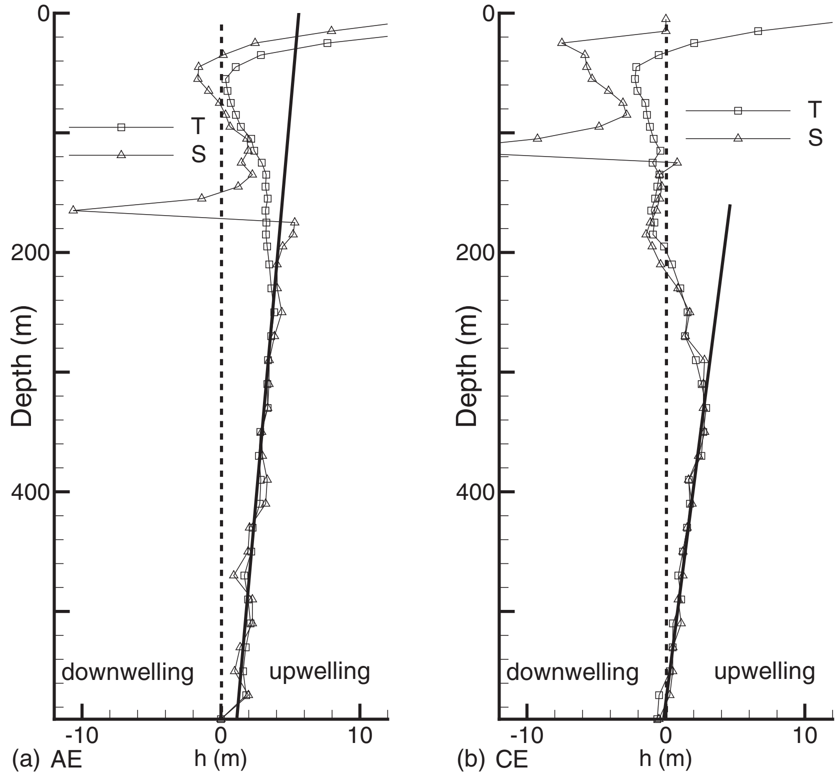

Figure 11. The upwelling distances of temperature and salinity in the (a) AEs and (b) CEs.

air-sea flux exchanges, entrainment, and vertical mixing were strongest, as shown in Figure 8. The deeper the water, the closer the two T-S curves. In the thermocline (200 m deeper), the posttyphoon T-S curves overlap on the pretyphoon T-S curves (Figure 10b). The overlaps of T-S curves indicate that they are the same water mass with adiabatic motion. The observed temperature and salinity changes (Figure 9) below subsurface water are only due to the upwelling and/or downwelling of the water.

The method in *Sun et al*. [2012] is applied to the pretyphoon and posttyphoon profiles to calculate the upwelling distance. Both temperature and salinity profiles are used to calculate the depth independently. For example, the temperature profiles pretyphoon and posttyphoon are $T_1(d)$ and $T_2(d)$, respectively, where d is the depth below the sea surface. If $T_1(d)=T_2(d-h)$, then the water at depth of d has an upwelling height of h for temperature. Positive h represents upwelling while negative value means downwelling. The calculation of h for salinity is similar to the temperature but with more cautions. Since salinity change is not monotonic with depth, the calculated depth might be invalid at salinity maximum or minimum. When the water mass involves upwelling only, the distance from temperature should be identical to that from salinity.

The calculated upwelling distances are shown in Figure 11. The upwelling distances calculated with temperature and salinity are presented with squares and triangles, respectively. In the AEs, two curves were apart from each other from surface to subsurface water of 200 m depth (Figure 11a). The unexpected value h for salinity at 180 m depth partly is due to the local salinity maximum. The responses of water subsurface (0–170 m) depth in the AEs (Figure 8) should be dominated by nonadiabatic processes as vertical mixing. Below 180 m depth, two curves approximately overlapped within the thermocline, which means that the adiabatic motion of upwelling dominated the changes within the upper ocean in Figure 9.

The upwelling distance h was largest ($\sim$4 m) at the top of thermocline (200 m depth). It decreased linearly with depth (black line in Figure 11a). Such phenomenon was previously observed by Argo floats, when the ocean response time was a few days after typhoon forcing [*Sun et al*., 2012]. As time went on, the upwelling signal might be propagated with 2 m/h down to the deep ocean, until the whole column reaches to the same h [*Sun et al*., 2012]. The final steady state h can also be derived from SLA changes as noted before [*Shay et al*., 2000; *Sun et al*., 2012].

In the CEs, two curves were apart from each other from surface to subsurface water above 120 m depth similar to those in the AEs (Figure 11b). The responses of upper water (0–120 m depth) in the CEs (Figure 8) should be dominated by nonadiabatic processes as vertical mixing. Below 120 m depth, two curves approximately overlapped to the whole thermocline, which means that the adiabatic motions dominated the changes within the upper ocean in Figure 9. It is notable that such adiabatic motions include both upwelling (positive *h*) at the upper ocean with the largest value ($\sim$3 m) at 300 m depth and downwelling (negative *h*) at subsurface.

Although downwelling phenomenon was often observed far from typhoon center [e.g., *Price*, 1981; *Cheng et al.*, 2015], such phenomenon was only reported in the AEs [*Jaimes and Shay*, 2015] and was rarely observed in the CEs before.

3.5. Convergence and Divergence

Although there is generally an upwelling response to typhoon forcing in both AEs and CEs, the responses at subsurface ocean water are quite different in the AEs from CEs. In the AEs, there is divergence of the warm and fresh water at the subsurface, which can be concluded from the following facts. First, the water below subsurface upwells a few meters after typhoons. Part of the upper warm and fresh water within subsurface moved out the AEs. Second, the huge subsurface heat content loss in the AEs could not be balanced by the local air-sea interaction. The outflow of warmer water was the only source that could balance the heat content loss. Third, the outflow of surface fresher water from top and inflow of saltier water from bottom explained the calcification of subsurface after typhoon.

On the other hand, there is additional convergence of warm and fresh water against the upwelling at subsurface ocean in the CEs. First, the water at the bottom of subsurface downwelled a few meters after typhoons. Part of the cold and salt water at the bottom of subsurface consequently moved out the CEs. Second, the inflow of warmer and fresher water from the AEs explained the observed heat content gain and salinity loss at subsurface in the CEs after typhoons.

The scheme of the responses of the water below the subsurface in the AEs and CEs to typhoon forcing can be shown in Figure 12. The nonadiabatic processes, e.g., mixing and adiabatic processes, e.g., upwelling near the surface are not drawn in this figure, which are similar in both AEs and CEs. The responses below subsurface may be different for AEs and CEs. In the AEs, the outflow (red solid arrows) of warm and fresh water diverges at subsurface, while the inflow (red dashed arrows) of the water converges at subsurface in the CEs. Figure 12 extended the previous schematic diagram of vertical structure responses in the CEs [e.g., *Sun et al.*, 2012, 2014].

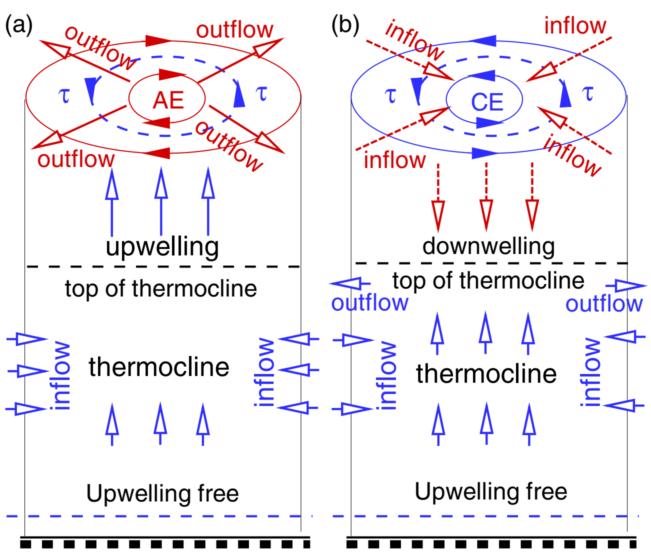

Figure 12. The schematic diagram of responses below the subsurface in the (a) AEs and (b) CEs, where τ represents the typhoon forcing. The complex processes above the subsurface are not drawn in this figure.

3.6. Large-Scale Mass Transport

Recent case studies found that typhoon could modulate the large-scale flow, e.g., the Kuroshio via cold eddy intensification [*Sun et al.*, 2009; *Wang et al.*, 2009], which in turn influence the typhoon [*Zhang et al.*, 2014]. The typhoon could influence large-scale mass transport in varies ways: directly wind stress curl input to ocean, vertical mixing, vertical and horizontal motions (convergence/divergence). In this paper, only the vertical motion inducing mass transport is estimated.

The divergence-convergence flow at subsurface by typhoon forcing can induce shallow overturning S_o between different eddies:

$$S_o = -\frac{\pi}{4} w_h D^2 \tag{6}$$

where w_h is the upwelling velocity and D is the diameter of eddy. The average diameter of eddies is 200 km, and that the annual average upwelling velocity ($w_h = 1.25 \times 10^{-7}$ m/s) is estimated as 4 m upwelling within 1 year. This contributes about 0.001 Sv mass transport for each eddy. On average, there are 21.4 typhoons each year in the WNPO (Figure 2). Suppose that each typhoon could influence 3 warm eddies during its lifetime. The estimated total mass transport is about 0.6 Sv due to typhoon forcing in each year.

According to the mass transport based on Sverdrup theory [*Thomas et al.*, 2014]:

$$\mathrm{S_v} = -\frac{\mathrm{f}}{\beta} \mathrm{w_h D}$$

where f is the Coriolis parameter and β is the beta effection. Suppose that eddies located at latitude 20°N, it contributes about 0.06 Sv mass transport for each eddy. The total mass transport in the WNPO is estimated to be about 4 Sv due to annual typhoon forcing, which is about 10 times of total mass transport (0.4 Sv) in the South China Sea [Wang et al., 2009]. This is also about 5–10% of total contribution to the mass transport (~40–60 Sv) by the Kuroshio. A similar result was obtained at the Taiwan Strait, where the monthly mean transport is reduced due to typhoon forcing by up to 0.45 Sv (more than 10% of total value) [*Zhang et al.*, 2014]. The typhoon activity play a role on large-scale mass transport.

The horizontal convergence/divergence also transported heat/salt from one eddy to another. For example, at least 80% of the total upper ocean heat loss (250 MJ/m^2) in the AEs is transported out to surrounding regions, which may significantly modulate the surrounding heat/salt distributions, and therefore contribute to large-scale heat transport [*Sriver and Huber*, 2007; *Cheng et al.*, 2015].

4. Discussion

4.1. Comparison With Recent Studies

In recent years, two-dimensional composite analyses are employed to ocean thermal structure response to typhoon forcing. By ignoring the eddies, the max average of SST change in cooling area within 3 days was about −1.4°C [*Wang et al.*, 2016]. But the max average of SST change (including both cooling and warming) within the same period dropped to a relatively smaller value of −0.8°C (from −0.5°C to −1.1°C depending on the wind forcing strength) [*Cheng et al.*, 2015]. The present values are relatively smaller as shown in Tables 1 and 2.

There are several possible reasons for this difference. The first one is that the previous ones were averages of the along track direction data while the present value is average of all the horizontal data. So the present values are reasonably smaller than the max values. The second reason might be the sampling time period. The timescale is also essential when we discuss the ocean responses. At first (especially very shortly after typhoon's passage), there is entrainment/upwelling near surface which induce SST cooling. Then the surrounding warming water converges into subsurface to supply the upwelled water from subsurface due to continuity [e.g., *Sun et al.*, 2012; *D'Asaro et al.*, 2014]. The longer the period is the smaller the cooling tends to be. The max average of SST change in cooling area within 10 days dropped to −1.0°C [*Wang et al.*, 2016], whereas the max average of SST change within 4–20 days dropped to −0.2°C [*Cheng et al.*, 2015]. The present investigation used average within 10 days after typhoon passing, the cooling values should be reasonably smaller. And other reasons (e.g., the strength of typhoon forcing) might also be involved. We also expect that there would be more observation data to reveal the full spatial-temporal response process in future.

Although the absolute values are smaller in this study, the results are similar. In previous studies, about 43% (−0.6°C) of total SST cooling (−1.4°C) was compensated by warming water in the forced region including both the AEs and the CEs. As for a further result, the warming water compensated about 52% (−0.45°C) of total SST cooling (−0.86°C) in CEs and 34% (−0.21°C) of total SST cooling (−0.62°C) in AEs according to the present study. It implies that the SST cooling induced by the typhoon in the CEs was compensated much more easily by warming water from AEs, as there are more AEs in WNPO (Figure 1).

4.2. Biomass Response

The subsurface upwelling and associated horizontal convergence/divergence can also modulate the biomass responses in the ocean in other ways. There was a disagreement on typhoon's contribution to integrated phytoplankton bloom [*Lin et al*., 2003; *Babin et al*., 2004; *Hanshaw et al*., 2008]. It was estimated that the typhoon-induced phytoplankton blooms may contribute as high as 20–30% of total annual new production in the SCS [*Lin et al*., 2003; *Sun et al*., 2010; *Zhao et al*., 2017] and threefold in the North Atlantic [*Babin et al*., 2004]. But *Hanshaw et al*. [2008] found the integrated impact of typhoons on sea surface phytoplankton bloom was only 1% of total annual new production in the North Atlantic. The underestimated results of *Hanshaw et al*. [2008] were because of the assumption that the phytoplankton response is contained within a swath from 1° to the left of the typhoon's center to 2° to the right and within a time period of 2 weeks [*Yang et al*., 2010; *Foltz et al*., 2015 and references therein]. Under this assumption, phytoplankton changes due to horizontal advection were not considered. Using the much larger boxes (from $3^\circ \times 3^\circ$ box to $4^\circ \times 4^\circ$ box), the integrated phytoplankton bloom due to typhoons increased significantly [*Foltz et al*., 2015; *Mei et al*., 2015]. The results in this study suggest that in order to include the influence of horizontal convergence/divergence on phytoplankton response, a larger area need to be considered.

Since the surface water is warm and oligotrophication in WNPO, especially in the AEs, the inflow of surface water from AEs suppresses not only the surface cooling but the phytoplankton blooms in CEs. This might be one of the reasons why the observed strong surface cooling events and phytoplankton blooms were much less than the numerical simulation expected.

5. Summary

Based on the SLA data and Argo data, the responses of the upper ocean (0–600 m depth) within the CEs and AEs to typhoon forcing in the WNPO were investigated. At the surface (0–10 m depth), more than half of Argo profiles had a strong cooling in the CEs, but some of them warmed due to intrusion of surrounding warm water. While in the AEs, most of the Argo profiles had a relatively weaker cooling comparing with that in CEs. In consequence, the average SST cooling is almost the same in AEs and CEs.

At the subsurface (10–200 m depth), there is a strong but shallow cooling in the CEs, weak but deep cooling in the AEs. The entrainment of surface warm water down to the middle of subsurface, which leads to warming of subsurface water in the CEs. While in the AEs, there is a notable cooling within whole subsurface layer due to the heat loss to air and the upwelling of deep cold water. There is weak cooling at the thermocline (200–600 m depth) in both of the AEs and the CEs.

The budgets of the heat and salinity are calculated for surface, subsurface, and thermocline. The whole upper ocean water column (0–600 m depth) had huge heat lost in the AEs (-250 MJ/m^2) and CEs (-45 MJ/m^2), which cannot be simply balanced by local air-sea flux lose. With T-S plots, both the vertical dynamic processes and horizontal advection are diagnosed from the data. The scheme of the responses in the AEs and CEs is presented. It is found that the AEs play as a divergence of warm and fresh water. As the water below subsurface upwells a few meters after typhoons, part of warm and fresh water at the top of subsurface diverge out of eddies after typhoons. On the other hand, the warm and fresh water converges to subsurface in the CEs, then downwells to thermocline. The convergence of warm water partly suppresses the cooling and the phytoplankton blooms near surface in the CEs.

Consequently, there is the secondary cooling center occurred at a much shallow layer of 100 m due to upwelling of deep cold water in the AEs. While in the CEs, the secondary cooling center locates at a much deep layer of 350 m depth as downwelling of warm water depressing the upwelling deep cold water. These two secondary cooling centers in the AEs and CEs agree with the recent finding of weak cooling centers at 100 and 350 m. This shallow divergence-convergence flow could lead to a relatively nonlocally shallow overturning flow in the upper oceans. The deep upwelling could contribute the large-scale mass and heat transport. These may potentially influence the large-scale ocean circulations, biomass responses, and climates.

AGU Journal of Geophysical Research: Oceans 10.1002/2017JC012814

Acknowledgments

We thank the anonymous referees for their comments and suggestions. This work is supported by the National Basic Research Program of China (2013CB430301 and 2013CB430303), the National Foundation of Natural Science of China (41376017), the National Programme on Global Change and Air-Sea Interaction (GASI-IPOVAI-04 and GASI-IPOVAI-06), and the Open Fund of State Key Laboratory of Satellite Ocean Environment Dynamics (SOED1501). The eddy detection method and the code can be downloaded (http://www.ocean-sci.net/12/1249/2016/). We thank the Joint Typhoon Warning Center (JTWC) for providing typhoon track data (http://www.usno.navy.mil/JTWC/), AVISO for SLA data (http://www.aviso.oceanobs.com/), national geophysical data center for ocean depth data (http://rda.ucar.edu/datasets/ds759.2/), APDRC/IPRC for surface currents data (SUCD) (http://apdrc.soest.hawaii.edu/projects/SCUD/), and China Argo Real-time Data center for float profiles (http://www.argo.org.cn/english/).

References

Babin, S. M., J. A. Carton, T. D. Dickey, et al. (2004), Satellite evidence of hurricane–induced phytoplankton blooms in an oceanic desert. *J. Geophys. Res.: Oceans*, *109*, C03043, doi:10.1029/2003JC001938.

Bennett, A. F., and W. B. White (1986), Eddy heat flux in the subtropical North Pacific, *J. Phys. Oceanogr.*, *16*(4), 728–740, doi:10.1175/1520-0485(1986)016<0728:EHFITS>2.0.CO;2.

Chelton, D. B., P. Gaube, M. G. Schlax, J. J. Early, and R. M. Samelson (2011), The influence of nonlinear mesoscale eddies on near-surface oceanic chlorophyll, *Science*, *334*(6054), 328–332, doi:10.1126/science.1208897.

Cheng, L., J. Zhu, and R. L. Sriver (2015), Global representation of tropical cyclone-induced short-term ocean thermal changes using Argo data, *Ocean Sci.*, *11*, 719–741, doi:10.5194/os-11-719-2015.

D'Asaro, E. A., et al. (2014), Impact of typhoons on the ocean in the Pacific: ITOP, *Bull. Am. Meteorol. Soc.*, *95*, 1405–1418, doi:10.1175/BAMS-D-12-00104.1.

Dong, C., J. C. McWilliams, Y. Liu, and D. Chen (2014), Global heat and salt transports by eddy movement, *Nat. Commun.*, *5*, 3294, doi:10.1038/ncomms4294.

Foltz, G. R., K. Balaguru, and L. R. Leung (2015), A reassessment of the integrated impact of tropical cyclones on surface chlorophyll in the western subtropical North Atlantic, *Geophys. Res. Lett.*, *42*, 1158–1164, doi:10.1002/2015GL063222.

Greatbatch, R. J. (1984), On the response of the ocean to a moving storm: Parameters and scales, *J. Phys. Oceanogr.*, *14*, 59–77, doi:10.1175/1520-0485(1984)014<0059:OTROTO>2.0.CO;2.

Guan, S., W. Zhao, J. Huthnance, J. Tian, and J. Wang (2014), Observed upper ocean response to typhoon Megi (2010) in the Northern South China Sea, *J. Geophys. Res. Oceans*, *119*, 3134–3157, doi:10.1002/2013JC009661.

Hanshaw, M. N., M. S. Lozier, and J. B. Palte (2008), Integrated impact of tropical cyclones on sea surface chlorophyll in the North Atlantic, *Geophys. Res. Lett.*, *35*, L01601, doi:10.1029/2007GL031862.

Jaimes, B., and L. K. Shay (2015), Enhanced wind-driven downwelling flow in warm oceanic eddy features during the intensification of Tropical Cyclone Isaac (2012): Observations and theory, *J. Phys. Oceanogr.*, *45*, 1667–1689, doi:10.1175/JPO-D-14-0176.1.

Jaimes, B., L. K. Shay, and G. R. Halliwell (2011), The response of quasigeostrophic oceanic vortices to tropical cyclone forcing, *J. Phys. Oceanogr.*, *41*(10), 1965–1985, doi:10.1175/jpo-d-11-06.1.

Jing, Z., and L. Wu (2014), Intensified diapycnal mixing in the midlatitude western boundary currents, *Sci. Rep.*, *4*, 7412, doi:10.1038/srep07412.

Knaff, J. A., M. DeMaria, C. R. Sampson, J. E. Peak, J. Cummings, and W. H. Schubert (2013), Upper oceanic energy response to tropical cyclone passage, *J. Clim.*, *26*(8), 2631–2650, doi:10.1175/JCLI-D-12-00038.1.

Li, Q. -Y., and L. Sun (2015), Technical Note: Watershed strategy for oceanic mesoscale eddy splitting, *Ocean Sci.*, *11*(2), 269–273, doi:10.5194/os-11-269-2015.

Li, Q.-Y., L. Sun, S.-S. Liu, T. Xian, and Y.-F. Yan (2014), A new mononuclear eddy identification method with simple splitting strategies, *Remote Sens. Lett.*, *5*(1), 65–72, doi:10.1080/2150704X.2013.872814.

Li, Q.-Y., L. Sun, and S.-F. Lin (2016), GEM: A dynamic tracking model for mesoscale eddies in the ocean, *Ocean Sci.*, *12*(6), 1249–1267, doi:10.5194/os-12-1249-2016.

Lin, I.-I. (2012), Typhoon-induced phytoplankton blooms and primary productivity increase in the western North Pacific subtropical ocean, *J. Geophys. Res.*, *117*, C03039, doi:10.1029/2011JC007626.

Lin, I. I., W. T. Liu, C. C. Wu, G. T. F. Wong, C. Hu, Z. Chen, W. D. Liang, Y. Yang, and K. K. Liu (2003), New evidence for enhanced ocean primary production triggered by tropical cyclone, *Geophys. Res. Lett.*, *30*(13), 1718, doi:10.1029/2003GL017141.

Lin, I.-I., C.-C. Wu, I.-F. Pun, and D. S. Ko (2008), Upper ocean thermal structure and the western North Pacific category-5 typhoons, Part I: Ocean features and category-5 typhoon's intensification, *Mon. Weather Rev.*, *136*, 3288–3306, doi:10.1175/2008MWR2277.1

Liu, L.-L., W. Wang, and R.-X. Huang (2008), The mechanical energy input to the ocean induced by tropical cyclones, *J. Phys. Oceanogr.*, *38*, 1253–1266, doi:10.1175/2007JPO3786.1.

Lu, Z., G. Wang, and X. D. Shang (2016), Response of a pre-existing cyclonic ocean eddy to a typhoon, *J. Phys. Oceanogr.*, *46*, 2403–2410, doi:10.1175/JPO-D-16-0040.1.

McGillicuddy, D. J. (2011), Eddies masquerade as planetary waves, *Science*, *334*(6054), 318–319, doi:10.1126/science.1208892.

Mei, W., and C. Pasquero (2013), Spatial and temporal characterization of sea surface temperature response to tropical cyclones, *J. Clim.*, *26*, 3745–3765, doi:10.1175/JCLI-D-12-00125.1.

Mei, W., C. C. Lien, I. I. Lin, and S. P. Xie (2015), Tropical cyclone-induced ocean response: A comparative study of the South China Sea and Tropical Northwest Pacific, *J. Clim.*, *28*(15), 5952–5968.

Pascual, A., Y. Faugère, G. Larnicol, and P.-Y. Le Traon (2006), Improved description of the ocean mesoscale variability by combining four satellite altimeters, *Geophys. Res. Lett.*, *33*, L02611, doi:10.1029/2005GL024633.

Powell, M. D., P. J. Vickery, and T. A. Reinhold (2003), *Reduced drag coefficient for high wind* speeds in tropical cyclones, *Nature*, *422*(6929), 279–283, doi:10.1038/nature01481.

Pujol, M.-I., Y. Faugère, G. Taburet, S. Dupuy, C. Pelloquin, M. Ablain, and N. Picot (2016), DUACS DT2014: The new multi-mission altimeter data set reprocessed over 20 years, *Ocean Sci.*, *12*, 1067–1090, doi:10.5194/os-12-1067-2016.

Price, J. F. (1981), Upper ocean response to a hurricane, *J. Phys. Oceanogr.*, *11*, 153–175, doi:10.1175/1520-0485(1981)011<0153:UORTAH>2.0.CO;2.

Price, J. F., T. B. Sanford, and G. Z. Forristall (1994), Forced stage response to a moving hurricane, *J. Phys. Oceanogr.*, *24*(2), 233–260, doi:10.1175/1520-0485(1994)024<0233:FSRTAM>2.0.CO;2.

Schade, L. R., and K. A. Emanuel (1999), The ocean's effect on the intensity of tropical cyclones: Results from a simple coupled atmosphere–ocean model, *J. Atmos. Sci.*, *56*(4), 642–651.

Shay, L. K., G. J. Goni, and P. G. Black (2000), Effects of a warm oceanic feature on Hurricane Opal, *Mon. Weather Rev.*, *128*, 1366–1383, doi:10.1175/1520-0493(2000)128<1366:EOAWOF>2.0.CO;2.

Sriver, R. L., and M. Huber (2007), Observational evidence for an ocean heat pump induced by tropical cyclones, *Nature*, *447*(7144), 577–580, doi:10.1038/nature05785.

Sun, L., Y.-J. Yang, and Y.-F. Fu (2009), Impacts of typhoons on the Kuroshio large meander: Observation evidences, *Atmos. Ocean Sci. Lett.*, *2*, 45–50, doi:10.1080/16742834.2009.11446772.

Sun, J., L.-Y. Oey, R. Chang, F. Xu, and S. M. Huang (2015), Ocean response to typhoon Nuri (2008) in western pacific and south china sea, *Ocean Dyn.*, *65*(5), 735–749, doi:10.1007/s10236-015-0823-0.

Sun, L., Y.-J. Yang, T. Xian, Z.-M. Lu, and Y.-F. Fu (2010), Strong enhancement of chlorophyll a concentration by a weak typhoon, *Mar. Ecol. Prog. Ser.*, *404*, 39–50, doi:10.3354/meps08477.

Sun, L., Y.-J. Yang, T. Xian, Y. Wang, and Y.-F. Fu (2012), Ocean responses to Typhoon Namtheun explored with Argo floats and multiplatform satellites, *Atmos. Ocean*, *50*, 15–26, doi:10.1080/07055900.2012.742420.

Sun, L., Y.-X. Li, Y.-J. Yang, Q. Wu, X.-T. Chen, Q.-Y. Li, Y.-B. Li, and T. Xian (2014), Effects of super typhoons on cyclonic ocean eddies in the western North Pacific: A satellite data-based evaluation between 2000 and 2008, *J. Geophys. Res. Oceans*, *119*, 5585–5598, doi:10.1002/2013JC009575.

Thomas, M. D., A. M. De Boer, H. L. Johnson, and D. P. Stevens (2014), Spatial and temporal scales of Sverdrup balance, *J. Phys. Oceanogr.*, *44*(10), 2644–2660, doi:10.1175/JPO-D-13-0192.1.

Vincent, E. M., M. Lengaigne, G. Madec, J. Vialard, G. Samson, N. Jourdain, C. E. Menkes, and S. Jullien (2012), Processes setting the characteristics of sea surface cooling induced by tropical cyclones, *J. Geophys. Res.*, *117*, C02020, doi:10.1029/2011JC007396.

Vincent, E. M., G. Madec, M. Lengaigne, J. Vialard, and A. Koch-Larrouy (2013), Influence of tropical cyclones on sea surface temperature seasonal cycle and ocean heat transport, *Clim. Dyn.*, *41*(7), 2019–2038, doi:10.1007/s00382-012-1556-0.

Walker, N. D., R. R. Leben, and S. Balasubramanian (2005), Hurricane-forced upwelling and chlorophyll a enhancement within cold-core cyclones in the Gulf of Mexico, *Geophys. Res. Lett.*, *32*, L18610, doi:10.1029/2005GL023716.

Wang, G., J. Su, and P. C. Chu (2003), Mesoscale eddies in the South China Sea observed with altimeter data, *Geophys. Res. Lett.*, *30*(21), 2121, doi:10.1029/2003GL018532.

Wang, G., Z. Ling, and C. Wang (2009), Influence of tropical cyclones on seasonal ocean circulation in the South China Sea, *J. Geophys. Res.*, *114*, C10022, doi:10.1029/2009JC005302.

Wang, G., L. Wu, N. C. Johnson, and Z. Ling (2016), Observed three-dimensional structure of ocean cooling induced by Pacific tropical cyclones, *Geophys. Res. Lett.*, *43*, 7632–7638, doi:10.1002/2016GL069605.

Wang, Z. F., Q. Y. Li, L. Sun, S. Li, Y.-J. Yang, and S. S. Liu (2015), The most typical shape of oceanic mesoscale eddies from global satellite sea level observations, *Front. Earth Sci.*, *9*(2), 202–208, doi:10.1007/s11707-014-0478-z.

Wu, Q. Y., and D. Chen (2012), Typhoon-induced variability of the oceanic surface mixed layer observed by Argo Floats in the Western North Pacific Ocean, *Atmos. Ocean*, *50*(Suppl. 1), 4–14, doi:10.1080/07055900.2012.712913.

Xu, C., X. D. Shang, and R. X. Huang (2014), Horizontal eddy energy flux in the world oceans diagnosed from altimetry data, *Sci. Rep.*, *4*, 5316, doi:10.1038/srep05316.

Yang, Y.-J., L. Sun, Q. Liu, T. Xian, and Y.-F. Fu (2010), The biophysical responses of the upper ocean to the typhoons Namtheun and Malou in 2004, *Int. J. Remote Sens.*, *31*(17), 4559–4568, doi:10.1080/01431161.2010.485140.

Ye, H. J., Y. Sui, D. L. Tang, and Y. Afanasyev (2013), A subsurface chlorophyll a bloom induced by typhoon in the South China Sea, *J. Mar. Syst.*, *128*, 138–145, doi:10.1016/j.jmarsys.2013.04.010.

Zhang, H., D. Chen, L. Zhou, X. Liu, T. Ding, and B. Zhou (2016), Upper ocean response to typhoon Kalmaegi (2014), *J. Geophys. Res. Oceans*, *121*, 6520–6535, doi:10.1002/2016JC012064.

Zhang, W.-Z., F. Chai, H.-S. Hong, and H. Xue (2014), Volume transport through the Taiwan Strait and the effect of synoptic events, *Cont. Shelf Res.*, *88*, 117–125, doi:10.1016/j.csr.2014.07.010.

Zhang, Z., Y. Zhang, W. Wang, and R. X. Huang (2013), Universal structure of mesoscale eddies in the ocean, *Geophys. Res. Lett.*, *40*, 3677–3681, doi:10.1002/grl.50736.

Zhao, H., J. Pan, G. Han, A. T. Devlin, S. Zhang, and Y. Hou (2017), Effect of a fast-moving tropical storm Washi on phytoplankton in the northwestern South China Sea, *J. Geophys. Res. Oceans*, *122*, 3404–3416, doi:10.1002/2016JC012286.

Zheng, Z.-W., C.-R. Ho, Q. Zheng, Y.-T. Lo, N.-J. Kuo, and G. Gopalakrishnan (2010), Effects of preexisting cyclonic eddies on upper ocean responses to Category 5 typhoons in the western North Pacific, *J. Geophys. Res.*, *115*, C09013, doi:10.1029/2009JC005562.